



Role of potassium in the enhancement of the catalytic activity of calcium oxide towards tar reduction

Pavleta Knutsson^{a,*}, Valentina Cantatore^a, Martin Seemann^b, Pui Lam Tam^c, Itai Panas^a

^a Department of Chemistry and Chemical Engineering, Chalmers University of Technology, Kemigården 4, 41296 Gothenburg, Sweden

^b Department of Space, Earth and Environment, Chalmers University of Technology, Hörsalsvägen 7B, 41293, Gothenburg, Sweden

^c Department of Industrial and Materials Science, Chalmers University of Technology, Rännvägen 2A, 41296 Gothenburg, Sweden

ARTICLE INFO

Keywords:

Gasification
Catalyst
Olivine
Potassium role
Tar reduction
DFT

ABSTRACT

Gasification in fluidized bed systems is considered to be a highly promising alternative for the thermal conversion of biomass. A major challenge for this process is the formed tars, which represent a loss of energy from the product gas and entail additional costs for their removal. Olivine is considered to be the most effective catalytic bed material in terms of its impact on tar levels in the product gas. Additions and modifications to olivine have revealed the potential to enhance its catalytic activity. In the present study, the effect of the addition of K_2CO_3 to the gasification process on the tar decomposition capability of olivine were evaluated. The effect of the added K_2CO_3 on the product gas was assessed in the 30-MWth pilot gasification plant GoBiGas. Once decreases in the tar level were detected, samples of the bed material were extracted from the system and evaluated for morphological and chemical changes related to the observed catalytic effect. SEM-EDX and XPS analyses of the surfaces of the olivine particles indicate that the additive is involved in the formation of mixed oxides of Ca and K within the outermost layer of the olivine particles. DFT modeling showed that the formation of mixed Ca and K oxides changes the oxidation potential of the surface, which may explain the increased activity of ash-coated olivine towards tar reduction.

1. Introduction

Biomass represents the carbon-neutral alternative with the strongest potential to replace the fossil fuels currently used for heat and electricity generation, as well as for the production of fuels and chemicals [1]. Of the existing technologies, biomass gasification is considered to be one of the most cost- and energy-efficient [2]. During gasification, the biomass is converted to a product gas, which consists mainly of CO, CO_2 , H_2 and H_2O but also contains undesired byproducts, such as tars. Commonly, tars are defined as higher hydrocarbons (usually aromatic) that can condense on available surfaces during the process, thereby causing clogging in the system [3]. In addition to being problematic for plant operation, tars contain chemically bound energy, which can constitute up to 5% of the energy content of the fuel [4]. Therefore, lowering the tar yield not only decreases the need for gas cleaning, but also increases the quality of the final gas product.

There are at present two main ways to lower the tar yield: (i) limiting the formation of tar by removing the precursors for tar formation, which can be achieved by adjusting the reaction environment or enhancing the decomposition of already formed tar; and (ii) decomposition of already formed tar, for which catalytic decomposition using

specific bed materials and additives is the most effective alternative [5,6]. Different bed materials and additives have been tested over the years. The feature shared by the most commonly used alternatives is their calcium content. One of the first additives used in the gasification process and shown to influence the gas composition and the heating value was limestone ($CaCO_3$) [7]. Another Ca-containing catalyst that has gained popularity for tar reforming is dolomite ($CaMgCO_3$), which is also the most intensively studied in-bed additive. The addition to the biomass feed of as little as 3% of these calcium-containing catalysts results in a 40% reduction in the level of tar in the gas [8]. Calcium-containing additives mainly affect the high-molecular-weight hydrocarbons, while the outputs of benzene and methane are more or less unchanged, which has led to recommendations regarding the use of dolomite and limestone, mainly in connection with other metallic reforming catalysts [5]. A further limitation linked to the use of Ca-containing species directly in the process is their mechanical resistance, which may result in material breakage during operation and the formation of fines, which may disrupt the process and necessitate additional gas handling [7].

Alkali-containing species also increase the rate of the gasification process [9–12]. Alkali carbonates have been used as additives for

* Corresponding author.

E-mail address: pavleta.knutsson@chalmers.se (P. Knutsson).

enhancing coal and biomass gasification in several industrial processes, and their effects have been confirmed by several groups [13–16]. Different mechanisms have been proposed, ranging from the effect of alkali on the unzipping of the cellulose chains [17] to the potential for alkali carbonates to promote the formation of the liquid-surface interface [15]. Several published studies have suggested that the observed effects of alkalis are linked to oxygen transport to the tars, thereby facilitating their oxidation [18].

Currently, olivine (FeMgSiO_4) is the bed material of choice for dual fluidized bed (DFB) gasification plants [19–21]. It has been shown in multiple studies that for this material to perform optimally, an “activation” step is needed [22,23], which involves the formation of a coating layer around the bed material particles [24–27]. The coating has been shown by several groups (e.g., Kirnbauer et al. [28]) to consist of two layers: (i) an inner layer that is rich in calcium and potassium; and (ii) an outer layer in which calcium-containing species predominate. The role that this coating plays in tar decomposition has been attributed to the content of calcium oxide, as recently confirmed in a comparison of the activities of olivine and pure calcium oxide used as bed materials [29]. The potassium detected within the coating has not been assigned any significant role in promoting the catalytic activity of the bed material. The low levels of potassium detected have instead been linked to the high volatile content of alkali at the combustion and gasification temperatures, as well as to the low rate of potassium re-incorporation into the formed calcium silicates [28].

Analyses of the materials sampled from the GoBiGas reactor have revealed a correlation between the content of potassium in the calcium layer formed on the bed particles and the observed activities of the bed materials towards tar decomposition [30]. Considering the known effect of alkali on the surface oxidation of graphite [18] and the presence of alkali in the coatings formed on the bed material particles, there is a need to re-assess the roles of potassium and calcium incorporated in the formed coatings on the tar decomposition as well as to evaluate the possibility that potassium and calcium carbonates exert simultaneous triggering effect. In the present study, samples of bed material collected after the addition of K_2CO_3 to the GoBiGas gasifier, which led to a dramatic decrease in tar yield, were analyzed. The effects of the added alkali salt were evaluated with respect to chemical and morphological changes to the sampled bed material. The results for the migration of K and Ca in the bed particles were then combined with first-principles calculations using density functional theory (DFT), in order to build a hypothesis for the observed effects.

2. Experimental

2.1. GoBiGas gasification plant

The GoBiGas gasifier (Fig. 1, also described in [31]) is a 30-MW_{th} DFB gasifier that consists of two interconnected fluidized bed reactors. The fuel (composition listed in Table 1) is fed to the gasifier, which is a bubbling bed that is fluidized with steam, in which the fuel is partially converted to a product gas. The remaining char is converted with air in a circulating fluidized bed combustor, thereby providing the heat for the process. The product gas is cooled to recover heat and then cleaned before being synthesized into methane.

The operational conditions applied in the plant during the experimental campaign are summarized in Table 2.

Based on the analysis of the samples from the GoBiGas unit before the addition of K_2CO_3 the dominant tar components were benzene and three-ring and higher aromatic compounds (Fig. 2).

During the K-triggering (denoted as ‘activation’) campaign, 5 l/h of 40 wt% K_2CO_3 solution was injected into the combustor side of the unit. Upon the addition of K_2CO_3 , an almost two-fold decrease in all the tar species was observed. An increase in the H_2/CO ratio was also observed in the experiments involving olivine aging, although the final value for the H_2/CO ratio in the present case (2.4) was significantly higher than

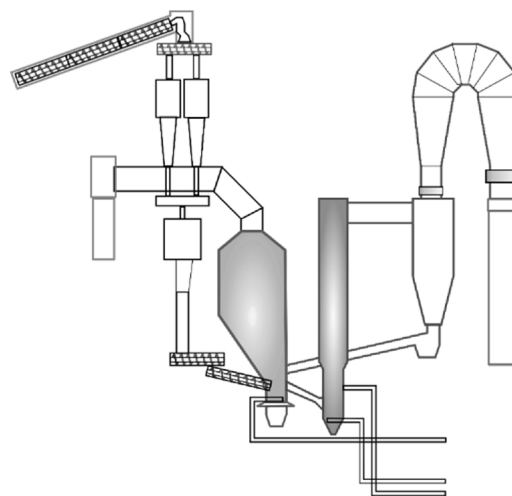


Fig. 1. Schematic of the GoBiGas unit, with highlighting (shading) of the gasifier (left side) and combustor (right side) components [30].

Table 1

Fuel analysis (based on fuel as-received).

Parameter	Value	Unit
Moisture	1.5	%
Ash content	0.4	%
Volatiles content	82.4	%
C	49.9	%
O	43.1	% (calculated)
H	6.5	%
N	< 0.1	%
S	< 0.010	%
Cl	< 0.010	%
Ca	950	mg/kg
K	520	mg/kg
Mg	170	mg/kg
Fe	42	mg/kg
Al	26	mg/kg
Si	< 510	mg/kg
Na	< 51	mg/kg

Table 2

Operational parameters used during the test runs in the GoBiGas gasifier.

Bed inventory	Temperature in the bed, gasifier [°C]	Fuel flow, [kg daff/h]	Fluidization level [kg steam/h]	Temperature in the combustor [°C]
Calcined Serpentine	870	4600	2300	960

that obtained through olivine aging in previous studies [32].

It should be noted that deposition of K was not observed either on the heat exchangers during the performed test or during the follow-up K_2CO_3 activation of the bed material.

2.2. Materials

Olivine, which is a silicate mineral with the general formula $(\text{Mg}^{2+}, \text{Fe}^{2+})_2\text{SiO}_4$, belongs to a larger group called the olivine group, with fayalite (iron-rich) and forsterite (magnesium-rich) minerals as the end-members [33]. In the present study, a serpentine that was calcined prior to use and delivered from Austria was used. The main mineral phases in the used material are listed in Table 3. Samples were taken from the gasifier using a water-cooled probe during operation of the reactor and cooled inside the probe before being exposed to air. The bed material

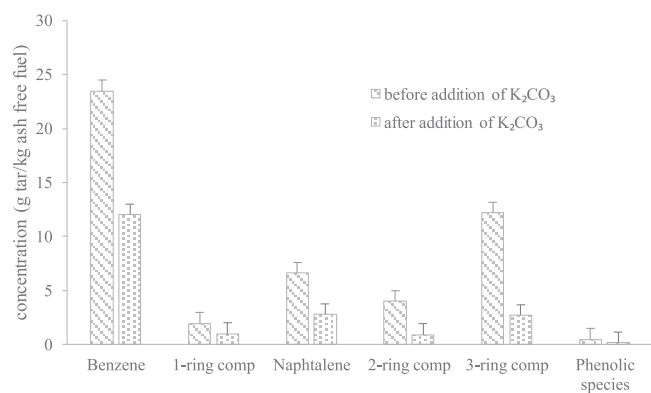


Fig. 2. Levels of tar components in the GoBiGas unit during the measurement campaign prior to and following the addition of K₂CO₃ (8 h post-injection).

Table 3

Composition of the olivine used as bed material in the GoBiGas gasifier.

	Weight percentages
MgO	48.90
SiO ₂	41.00
Fe ₂ O ₃	9.50
Al ₂ O ₃	0.30
CaO	0.13
Cr ₂ O ₃	0.57
NiO	0.30
MnO	0.12
Na ₂ O	0.02
K ₂ O	0.01
L.O.I.	0.00

inventory was 15 tonnes and consisted of olivine with a particle size distribution of 180–500 µm with an estimated circulation rate of 65 kg/h.

2.3. Analytical techniques

Samples of the olivine bed were extracted and analyzed for changes in the total elemental composition, as well as in the elemental distribution.

For the total elemental composition analysis, the collected bed samples were initially dissolved in LiBO₂ using a microwave oven to dissolve the samples through several heat treatment steps, and further analyzed using ICP-AES according to the EN 13,656 standard.

The crystalline phase characterization of all the materials was performed in an x-ray powder diffractometer (XRD, Siemens D5000 with CuK_α characteristic radiation). A step size of 0.05° and an extracted profile in the range of 20°–90° (2θ) were used.

The bed material particles were immobilized in epoxy resin and ground to obtain a flat cross-section of the particles. Scanning Electron Microscopy coupled with Energy Dispersive x-ray Spectroscopy (SEM-EDS) was used for the morphological evaluation of the material, as well as for elucidating the elemental distributions within the particles. Tabletop Phenom ProX and Quanta 200FEG equipped with an Oxford EDS were the systems of choice for the evaluations. Both systems were used in low-vacuum mode and with charge reduction. During the EDS analysis, point analyses and intensity maps were used to derive the elemental distributions.

The Brunauer–Emmett–Teller (BET) surface area was determined by N₂ adsorption in the Micromeritics ASAP-2000 equipment. The obtained values for all the materials were in the range of 1.90–2.08 m²/g.

A PHI 5000 VersaProbe III – Scanning XPS Microprobe equipped with a focused monochromatic aluminum x-ray source with photon energy of 1486.6 eV and x-ray beam size of 100 µm was used for the

surface analysis. In the chemical state evaluation using binding energy (BE) analysis, a correction was made by aligning the peak positions with reference to the standard adventitious carbon peak (C1s) at 284.6 eV [34].

The XPS results confirmed the previous EDS and XRD findings regarding the presence of K, Ca, Fe and O in the outermost layer of the bed particles. In the first 50 nm of the layer, the compositional ratio of K:Ca:Si changed from 2:1:1 to almost 1:1:1 across the analyzed cross-section. Surface contaminants, mostly carbon (C), were removed by etching using argon ion sputtering; a shift of 0.2 eV was applied for the BE evaluation of all the elements based on the C1s peak after etching. To understand the state of the discovered K and Ca, the fitted peaks of O1s and K2p and Ca2p were used.

2.4. Theoretical calculations

The CASTEP software package [35] within the Material Studios framework [36] was utilized, and the PBE GGA functional program [37] was employed for all the spin-polarized calculations. Core electrons were described by the ultrasoft pseudopotentials [38] in conjunction with a cut-off energy of 300 eV. The structures presented in this work have all been optimized while the lattice parameters have been held constant. The k-point sampling of the Brillouin zone was performed according to the Monkhorst–Pack scheme [39], with a 1 × 3 × 1 k-points mesh.

3. Results and discussion

3.1. Bed material analysis

Bed material characterization was used to identify those changes in the material structure and the elemental distribution that were induced by potassium addition to the gasifier bed.

The total elemental analysis of the bed materials obtained through acid digestion is presented in Fig. 3.

During the K-triggering experimental campaign week, the elemental compositions of the particles were independent of the added potassium and stable regardless of the period of exposure to K₂CO₃. The level of calcium stored in the particles increased with time, which is in agreement with the results of the analyses of previously sampled bed materials collected under the standard operational conditions at the plant. The previously shown decrease in tar levels (Fig. 2) occurred 8 h after the first bed sampling time-point. There was no statistically significant change in the potassium content associated with the K₂CO₃ injection. Thus, there was no clear evidence of a dependency of the observed catalytic activity on the total potassium content.

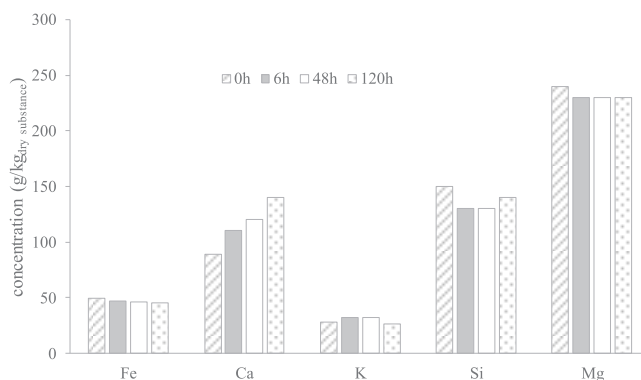


Fig. 3. Total amounts of calcium, potassium, iron, magnesium and silicon in the bed material samples collected from the GoBiGas gasifier at four different time-points (i.e., prior to K₂CO₃ injection and at 6 h, 48 h and 120 h after K₂CO₃ injection).

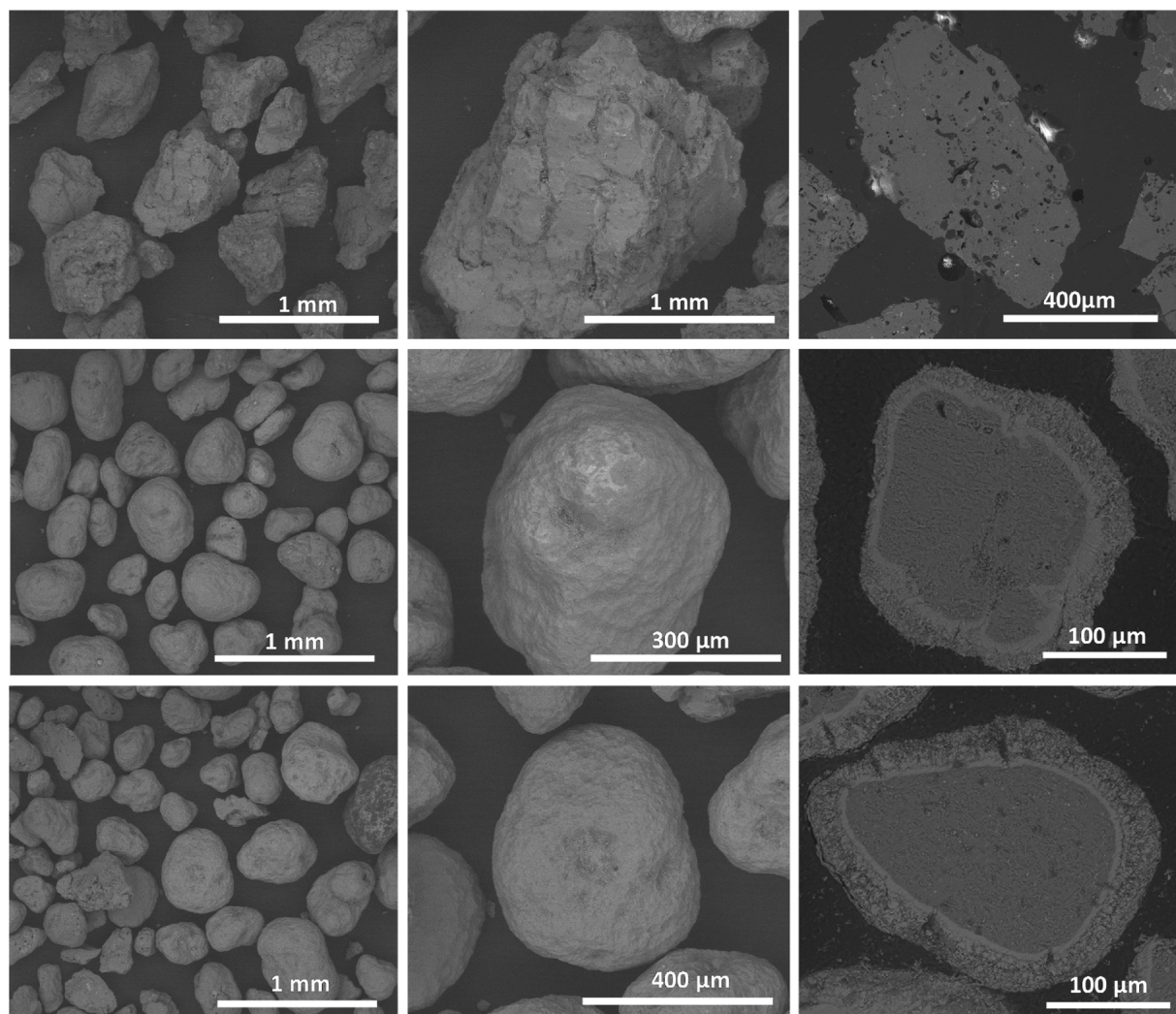


Fig. 4. Electron micrographs of bed material particles before exposure (first row) and bed particles sampled before and after the addition of K_2CO_3 (second and third rows, respectively). From left to right, the micrographs represent: overview image of the particles; overview image of a single particle; and cross-sectional image of a particle.

3.1.1. Morphology of and elemental distribution within the formed layer

Overview micrographs and cross-sectional images of representative particles before their use in the gasifier and particles sampled during operation, before and after the addition of K_2CO_3 , were compared to understand the effect of the material morphology on the observed activity of the material. The electron micrographs are presented in Fig. 4.

In Fig. 4, it can be seen that, as a result of attrition and bed material-ash interactions, the particles that have been in the system have smoothed edges compared to the fresh particles. No increase in porosity was observed for the particles after the addition of K_2CO_3 (measured values of $1.90\text{--}2.08\text{ m}^2/\text{g}$), which may explain the noted catalytic activity of the bed material. The formation of an ash layer around the particles is a well-known phenomenon. In the present case of using an olivine bed material, the coating layer, as previously described in our own studies [30], as well as by other groups [24], was formed already prior to K_2CO_3 addition (second row, Fig. 4). The added K did not change the morphology of the layer (third row, Fig. 4) but instead altered its chemical content. Examination of the micrographs of the layer could not reveal the “active” particle based just on the particles morphology.

Cross-sectional images of the bed material particles, sampled before and after the addition of K_2CO_3 (once a decrease in tar levels was noted) were then analyzed to follow the potassium distribution within the formed layers. Fig. 5 presents the EDS elemental intensity maps of Ca, Mg, Si and Fe, along with an elemental depth profile of a bed material

particle after K_2CO_3 addition. It should be noted that no statistically significant change was observed between the elemental distributions of Ca, Mg, Si and Fe before and after K_2CO_3 addition. The main difference observed after the addition of K_2CO_3 was for the potassium signal detected in the outermost part of the ash layer. Potassium enrichment of the outer part of the layer did not significantly alter the thickness of the layer.

From the cross-sectional image, it is clear that the formed coating consists of two sub-layers – a dense inner layer and a porous outer layer. Within the outer layer lies a morphologically compact outer sub-layer. From the EDS intensity map, it can be seen that the dense outermost area is rich in K, while the porous layer of the formed coating is Ca- and K-enriched. No K was detected outside the layer within the particle, implying that the events triggered by the addition of K_2CO_3 are induced via the potassium stored in the coating. The simultaneous presence of Ca and K in the inner part of the layer has been shown in previous studies [30], in which K was also detected within the particles.

3.1.2. Crystalline phase content of the formed layer

K-phase was not detected in any of the samples, mainly due to the detection limit of the x-ray diffraction method (the level of K in the sample would have to be $> 4\text{ wt.}\%$). XRD analyses revealed the predominance in the materials of forsterite-phase $Mg_{1.83}Fe_{0.17}(SiO_4)$ and periclase, MgO, both before exposure and when sampled during operation of the gasifier. Low levels of enstatite, $Ca_{0.025}Mg_{0.73}Fe_{0.2}SiO_4$,

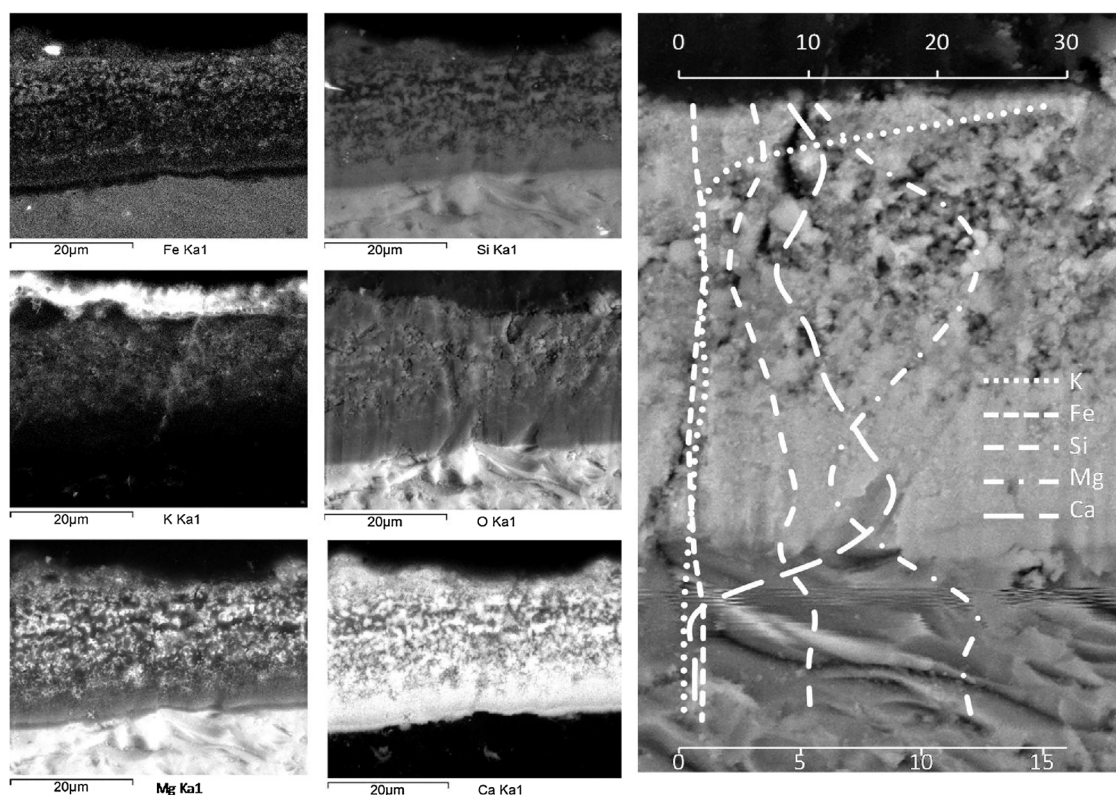


Fig. 5. Cross-sectional analyses of the particles sampled under operational conditions in the GoBiGas gasifier. Left to right: Fe, K, Mg, Si, O and Ca intensity EDS maps, showing the content of the layer and the co-presence of K and Ca in the outermost part of the coating layer. The depth elemental profiles confirm the preferential presence of K in the outermost layer.

and mixed calcium iron oxide, CaFe_2O_4 , were detected in the samples taken after the addition of K, which is in agreement with the elemental distribution observed through EDS (Fig. 5). These results suggest that the K-bearing phase is enclosed in the Ca-enriched zones identified in the layers and that the catalytically active sites consist of oxides of Ca and Fe.

Based on the thermodynamic calculations performed using FactSage [40], the most stable states of K_2CO_3 under gasification conditions are K_2O and KOH . From the XRD analysis of the calcium oxide phase and the EDS intensity maps showing the potassium distribution within the Ca-rich layer, the formation of a mixed K and Ca oxide can be assumed.

3.1.3. Chemical state of the constituents in the outermost part of the layer

To evaluate in greater detail the outermost layer of the coating which is in contact with the gas phase and can be expected to be the location of the catalytic activity, x-ray photoelectron spectroscopy (XPS) was performed. Fig. 6 shows the XPS spectra of the material.

The chemical states determined were consistent for all the analyzed depths. The positions located at 528.8 eV and 530.4 eV were determined to be metal oxide (for peak < 530.0 eV) and metal oxide/hydroxide (for peak > 530 eV), respectively [41]. The identification of the oxides was also consistent with the performed cation analysis.

Each K2p state was split into two sub-peaks: $2p_{3/2}$ and $2p_{1/2}$. The K2p peaks were fitted using two pairs. The K $2p_{3/2}$ positions were around 292.5 eV and 291.2 eV, respectively. They both refer to the K^+ state. The chemical entity at 292.5 eV was identified as a K^+ ion bonded to a simple anion-like oxide or halide (e.g., F^- , Cl^- , I^- , Br^-) [42]. No relevant match was found for the peak at 291.2 eV. K^+ bonded with a complex anion, such as $\text{Cr}_2\text{O}_7^{2-}$ or PO_4^{3-} , can be found at around 292.0 eV [43–45]. Thus, it is postulated that the K^+ state at 291.2 eV is bonded with a complex anionic structure, for example silicate.

Similar to the other 2p peaks, the $2p_{3/2}$ – $2p_{1/2}$ splitting was applied to the Ca2p curve-fitting. The fitted Ca2p spectra showed two chemical

states, at 345.2 eV and 346.2 eV, corresponding to Ca° [12] and Ca^{2+} in CaO [13]. The presence of Ca° is not very likely. Ca in the form of $\text{Bi}_{1.99}\text{Sr}_2\text{Ca}_2\text{Cu}_3\text{O}_x$ was previously identified at a binding energy of 344.9 eV [46], which indicates the presence of a nonstoichiometric oxide such as CaFeSiO_4 instead. The mechanism for the replacement of Ca^{2+} in the olivine matrix and the formation of silicates of Mg, Ca and Fe has been previously described by Kuba et al. [47].

Therefore, based on the results from the binding energy fitted peaks in the XPS spectra, apart from the silicates of calcium, iron, and magnesium, which were also detected by the SEM-EDS analysis (Fig. 5), the formation of oxides of K and Ca could be determined.

3.1.4. Modeling of the found compounds and a possible mechanism

As the experimental results pointed to the formation of a mixed oxide of Ca and K, in order to evaluate the effects of the K-enrichments of the CaO scale, theoretical calculations were performed based on the coexistence of K and Ca within the same oxide structure and the effect of the formed phase on the oxidizing behaviors of the bed materials.

First-principles calculations using density functional theory (DFT) were applied. An assumption was made that the apparent catalytic impact of potassium is due to substitutional doping of CaO. To unravel the apparent catalytic activity of potassium in the calcium oxide matrix, the impact of substitutional doping was explored by replacing two nearest neighbor Ca^{2+} ions in the oxide surface with two K^+ ions (Fig. 7). Replacing two Ca^{2+} ions in the lattice with two K^+ ions implies the generation of an oxygen vacancy. The ability of the oxygen vacancy to activate the O_2 by binding it to the vacancy was quantified, as this would result in a hole doping of the oxygen-dominated valence band, i.e., the system as a whole would become activated. Having activated the system, the reactivity towards the oxidation of tar was then explored with ethylene used as the reference (as ethylene is an example of an olefin with pi-bonding).

Fig. 7 shows the envisaged catalytic cycle for CaO that is doped with K. The first step (I) implies the binding of an O_2 molecule under

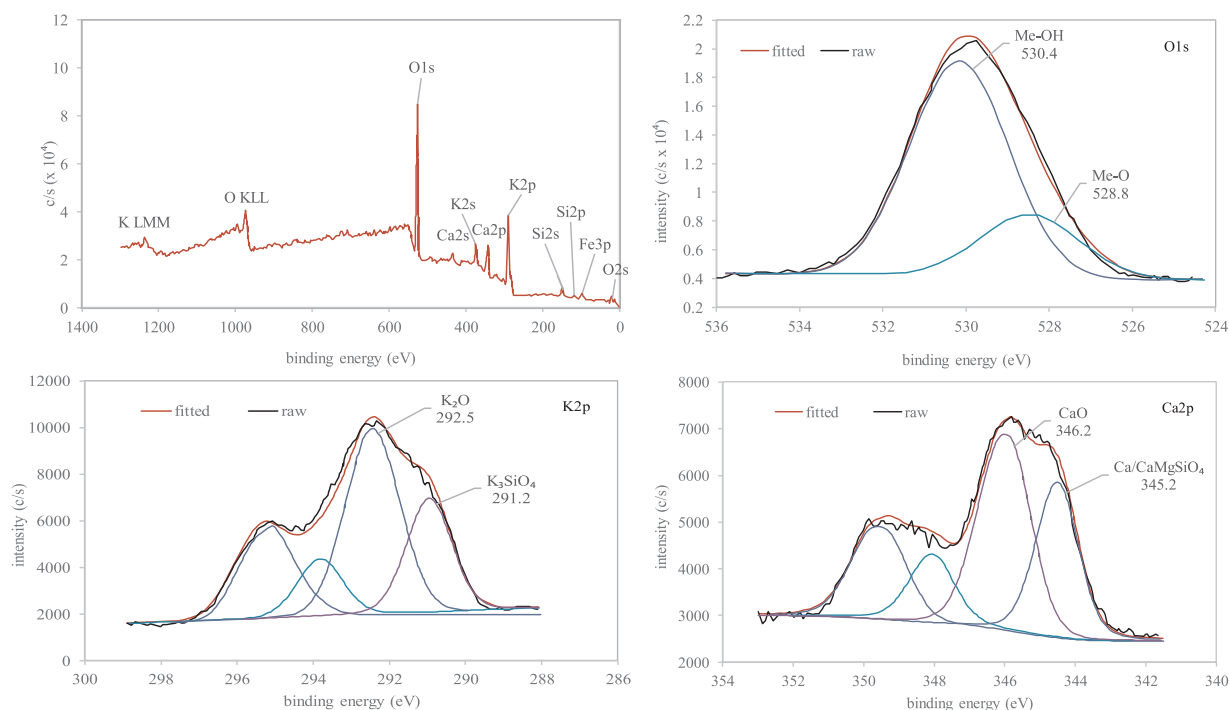


Fig. 6. XPS survey spectrum (top-left panel) and high-resolution XPS spectra showing the fitted O1s (top-right panel) K2p (bottom-left panel) and Ca2p (bottom-right panel) peaks.

oxidizing conditions (when the bed material is in the combustor) to the vacant site in the form of a peroxide ion, implying partial oxidation of the oxygen ions in the matrix. It should be noted that it is the availability of oxygen vacancy sites for O_2 accommodation that becomes the discriminating factor to initiate the catalytic cycle. The subsequent step (II) involves the oxidation of an ethylene molecule to ethylene oxide by one of the two oxygen atoms of the $O_2^{2-}(\text{surf})$ species (under the reducing conditions present in the gasifier). When the first ethylene oxide is formed it leaves the second oxygen in the vacancy site. Due to steric hindrance, the probability that the residual oxygen ion residing in the vacancy site $O^{(2-d)-}(\text{site})$ will subsequently oxidize a second olefin once the peroxide has reacted is understood to be low. Instead, it is gratifying to note that the reaction between the mentioned $O^{(2-d)-}(\text{site})$ and the adjacent oxygen ion on the surface is exothermic or only slightly endothermic (step III). Thus, the resulting protruding $O_2^{2-}(\text{adjac})$ moiety facilitates the oxidation of a second ethylene (step IV), a reaction that in turn is always exothermic, thereby restoring the initial surface structure, including the oxygen vacancy at the dopant site. The importance of proximity to the dopant is emphasized by allowing the formation of a second peroxy site.

The internal consistency of the above-proposed working hypothesis and the corresponding catalytic mechanism was validated through further calculations. Size effects in conjunction with potassium doping were explored in two ways. First, the impact of the slab thickness for any cooperative size, together with the doping effect was considered by employing a four-layer slab and then repeating the calculations for a

two-layer slab. Second, the way in which size might affect the catalytic energy landscape was explored by considering the low-coordination oxygen ion sites that are frequently present at the edges of a mono-dimensional rod (see Fig. 7c). The results are summarized in Fig. 8 and Table 4. It is interesting to note that despite variations in the model catalyst and the numbers, all three models are qualitatively in agreement, thereby validating the robustness of the proposed catalytic mechanism whereby substitutional potassium doping of calcium oxide can be considered as being capable of activating molecular O_2 .

It should be emphasized that the binding of $O_2(g)$ to the oxygen vacancy site is the rate-limiting step, given the entropic cost at 850°–960 °C. The Gibbs energy of activation is of the order of 1.3 eV. However, it must be borne in mind that the non-catalyzed reaction would involve the same entropic cost, i.e., ~ 2 eV. As the direct oxidation of tar by $O_2(g)$ requires simultaneous breaking of O–O and C–C bonds for the formation the C–O–O–C, the ability of the heterogeneous catalytic pathway to stabilize the oxygen intermediate in a two-step reaction, without loss of activity, is what renders the proposed pathway beneficial. The development of a mixed oxide scale of K and Ca can thus be a part of the mechanism through which the surface becomes catalytically activated for oxidizing tars.

4. Conclusions

K_2CO_3 addition to the gasification process resulted in decreases in the levels of all the sampled components from the gas tars. The

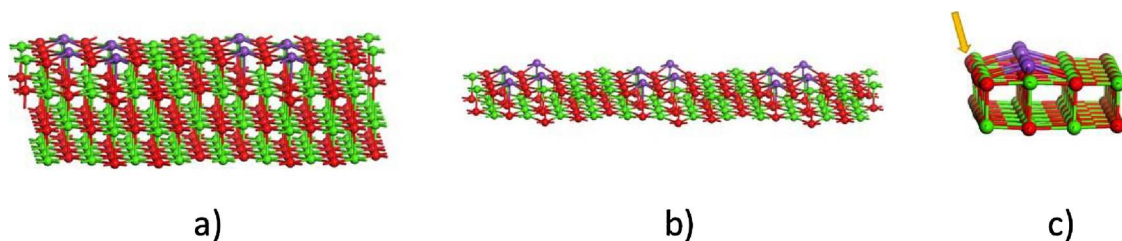


Fig. 7. CaO doped with K atoms. Color code: Ca, green; O, red; and K, purple. a) Four-layer slab; b) two-layer slab; c) monodimensional rod (the yellow arrow indicates the edge; see text for details). (For interpretation of the references to colour in this figure legend, the reader is referred to the web version of this article).

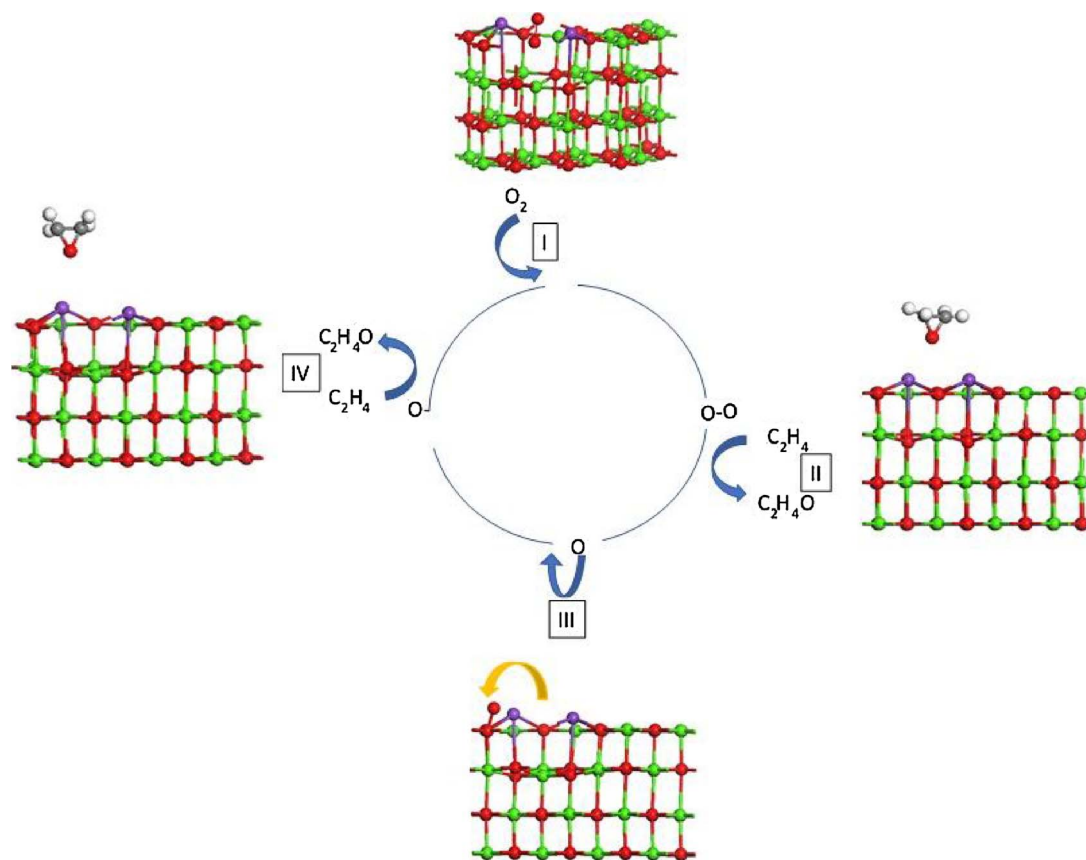


Fig. 8. Cycle showing the influence of K-doping on the oxidation of ethylene (as an example of an olefin with pi-bonding). The yellow arrow indicates the flipping of the oxygen atom in the vacancy site on the adjacent oxygen atom. (For interpretation of the references to colour in this figure legend, the reader is referred to the web version of this article).

Table 4

Energy values for steps I–IV of the catalytic cycle for a four-layer slab, two-layer slab, and a monodimensional rod.

STEP - Structure	Energy (eV)
I–four layers	–0.71
II–four layers	–0.53
III–four layers	–0.28
IV–four layers	–0.66
I–two layers	–0.94
II–two layers	–0.44
III–two layers	–0.13
IV–two layers	–0.67
I–rod	–0.69
II–rod	–0.49
III–rod	0.018
IV–rod	–1.02

formation of a layer that is enriched in Ca and consists of an outer and inner part was identified in the bed material, as observed in previous studies. The porosity of the layer could not be coupled to the observed tar decrease. Instead, enrichment of K in the outer layer and the formation of a mixed Ca and K oxide phase was detected through EDS and XRD. Using XPS analyses, it was found that the outermost layer, which is considered to be the catalytically active surface, consisted of K and Ca in the form of oxides. The activities of the K-inclusions in the CaO layer are explained by the formation of peroxy-type bonds that enhance the oxidizing behavior of the formed layer towards tars. A possible mechanism loop is proposed, with ethylene being used as a model compound, and the consistency and robustness of the proposed mechanism loop were validated through DFT calculations. Thus, through multiple experimental and modeling approaches, K-doped CaO could be identified as the catalytically active compound formed in the outer layer of

the bed material particles.

Acknowledgments

The Swedish Research Council (VR, 42034-1) and Swedish Gasification Center are acknowledged for their financial support.

References

- [1] A.V. Bridgwater, The technical and economic feasibility of biomass gasification for power generation, *Fuel* 74 (5) (1995) 631–653.
- [2] H. de Lasa, et al., Catalytic steam gasification of biomass: catalysts, thermodynamics and kinetics, *Chem. Rev.* 111 (9) (2011) 5404–5433.
- [3] T.A. Milne, et al., Biomass Gasifier “Tars”: Their Nature, Formation, and Conversion, National Renewable Energy Laboratory, 1999.
- [4] P. Tunå, H. Svensson, J. Brandin, Modeling of Reverse Flow Partial Oxidation Process for Gasifier Product Gas Upgrading, in *International Conference on Thermal Engineering: Theory and Applications 2010*, International Conference on Thermal Engineering: Marrakesh, Morocco, 2010.
- [5] D. Dayton, Review of the Literature on Catalytic Biomass Tar Destruction: Milestone Completion Report, in *Other Information: PBD: 1 Dec 2002*, (2002) p. Medium: ED; Size: 33 pages.
- [6] R.W.R. Zwart, Gas Cleaning Downstream Biomass Gasification – Status Report 2009, (2009).
- [7] L. Devi, K.J. Ptasinski, F.J.J.G. Janssen, A review of the primary measures for tar elimination in biomass gasification processes, *Biomass Bioenergy* 24 (2) (2002) 125–140.
- [8] I. Narváez, et al., Biomass gasification with air in an atmospheric bubbling fluidized bed. Effect of six operational variables on the quality of the produced raw gas, *Ind. Eng. Chem. Res.* 35 (7) (1996) 2110–2120.
- [9] S.J. Yuh, E. Wolf, FTIR studies of potassium catalyst-treated gasified coal chars and carbons, *Fuel* 62 (2) (1983) 252–255.
- [10] R. Fahmi, et al., The effect of alkali metals on combustion and pyrolysis of lolium and festuca grasses, switchgrass and willow, *Fuel* 86 (10) (2007) 1560–1569.
- [11] Y. Zhang, et al., Potassium catalytic hydrogen production in sorption enhanced gasification of biomass with steam, *Int. J. Hydrogen Energy* 39 (9) (2014) 4234–4243.
- [12] L.A. Hansen, et al., Influence of deposit formation on corrosion at a straw-fired

- boiler, *Fuel Process. Technol.* 64 (1) (2000) 189–209.
- [13] T. Suzuki, H. Ohme, Y. Watanabe, Alkali metal catalyzed carbon dioxide gasification of carbon, *Energy Fuel* 6 (4) (1992) 343–351.
 - [14] S.W. Lee, et al., The effect of Na₂CO₃ on the catalytic gasification of rice straw over nickel catalysts supported on kieselguhr, *Korean J. Chem. Eng.* 17 (2) (2000) 174–178.
 - [15] A.A. Lizzio, L.R. Radovic, Transient kinetics study of catalytic char gasification in carbon dioxide, *Ind. Eng. Chem. Res.* 30 (8) (1991) 1735–1744.
 - [16] N. Padban, PFB Air Gasification of Biomass, Investigation of Product Formation and Problematic Issues Related to Ammonia, Tar and Alkali, (2000).
 - [17] N. Padban, PFB Air Gasification of Biomass, Investigation of Product Formation and Problematic Issues Related to Ammonia, Tar and Alkali, Ingemar Odenbrand, Department of Chemical Engineering II, Lund University, 2000.
 - [18] D.W. McKee, D. Chatterji, The catalytic behavior of alkali metal carbonates and oxides in graphite oxidation reactions, *Carbon* 13 (5) (1975) 381–390.
 - [19] S. Rapagnà, et al., Steam-gasification of biomass in a fluidised-bed of olivine particles, *Biomass Bioenergy* 19 (3) (2000) 187–197.
 - [20] C. Courson, et al., Hydrogen production from biomass gasification on nickel catalysts: tests for dry reforming of methane, *Catal. Today* 76 (1) (2002) 75–86.
 - [21] L. Devi, K.J. Ptasinski, F.J.J.G. Janssen, A review of the primary measures for tar elimination in biomass gasification processes, *Biomass Bioenergy* 24 (2) (2003) 125–140.
 - [22] R. Rauch, et al., Comparison of different olivines for biomass steam gasification, *Proc Conf Science in Thermal and Chemical Biomass Conversion*, Victoria, Canada Conference (2004).
 - [23] L. Devi, K.J. Ptasinski, F.J.J.G. Janssen, Pretreated olivine as tar removal catalyst for biomass gasifiers: investigation using naphthalene as model biomass tar, *Fuel Process. Technol.* 86 (6) (2005) 707–730.
 - [24] F. Kirnbauer, et al., The positive effects of bed material coating on tar reduction in a dual fluidized bed gasifier, *Fuel* 95 (2012) 553–562.
 - [25] S. Kern, C. Pfeifer, H. Hofbauer, Reactivity tests of the water–gas shift reaction on fresh and used fluidized bed materials from industrial DFB biomass gasifiers, *Biomass Bioenergy* 55 (2013) 227–233.
 - [26] M. Kuba, F. Havlik, F. Kirnbauer, H. Hofbauer, Investigations on the Catalytic Activity of Bed Material Coating Regarding the Water-Gas-Shift Reaction and Steam Reforming of Model Compounds for Lighter and Heavier Hydrocarbons, in 23rd European Biomass Conference and Exhibition, Vienna, 2015, pp. 562–567.
 - [27] M. Kuba, et al., Influence of bed material coatings on the water-gas-shift reaction and steam reforming of toluene as tar model compound of biomass gasification, *Biomass Bioenergy* 89 (2016) 40–49.
 - [28] F. Kirnbauer, H. Hofbauer, Investigations on bed material changes in a dual fluidized bed steam gasification plant in güssing, Austria, *Energy Fuels* 25 (8) (2011) 3793–3798.
 - [29] M. Kuba, F. Kirnbauer, H. Hofbauer, Influence of coated olivine on the conversion of intermediate products from decomposition of biomass tars during gasification, *Biomass Convers. Biorefin.* 7 (1) (2017) 11–21.
 - [30] P. Knutsson, et al., Use of K₂CO₃ for the forced activation of olivine, *Fuel* (2017).
 - [31] A. Larsson, et al., Evaluation of performance of industrial-scale dual fluidized bed gasifiers using the chalmers 2–4-MWth gasifier, *Energy Fuel* 27 (11) (2013) 6665–6680.
 - [32] J. Marinkovic, Choice of Bed Material: a Critical Parameter in the Optimization of Dual Fluidized Bed Systems, Chalmers University of Technology, 2016.
 - [33] F.K. Lutgens, E.J. Tarbuck, *Essentials of Geology*, Prentice Hall, 2003.
 - [34] C.D. Wagner, G.E. Muilenberg, *Handbook of X-Ray Photoelectron Spectroscopy: a Reference Book of Standard Data for Use in X-Ray Photoelectron Spectroscopy*, Eden Prairie, Minn.: Physical Electronics Division, Perkin-Elmer Corp, 1979.
 - [35] S.J. Clark, et al., First principles methods using CASTEP, *Zeitschrift für Kristallographie* 220 (5/6) (2005) 567–570.
 - [36] *Material Studio 6.0 Accelrys Inc. Simulation Software, Material Studio 6.0.*
 - [37] J.P. Perdew, K. Burke, M. Ernzerhof, Generalized gradient approximation made simple, *Phys. Rev. Lett.* 77 (18) (1996) 3865–3868.
 - [38] D. Vanderbilt, Soft self-consistent pseudopotentials in a generalized eigenvalue formalism, *Phys. Rev. B* 41 (11) (1990) 7892–7895.
 - [39] H.J. Monkhorst, J.D. Pack, Special points for brillouin-zone integrations, *Phys. Rev. B* 13 (12) (1976) 5188–5192.
 - [40] C.W. Bale, et al., FactSage thermochemical software and databases, *Calphad* 26 (2) (2002) 189–228.
 - [41] J.-C. Dupin, et al., Systematic XPS studies of metal oxides, hydroxides and peroxides, *Phys. Chem. Chem. Phys.* 2 (6) (2000) 1319–1324.
 - [42] V. Nefedov, Y.A. Buslaev, Y.V. Kokunov, X-ray electron spectroscopy of alkali metal fluorides and alkaline earth metal fluorides, *Zhurnal Neorganicheskoi Khimii* 19 (5) (1974) 1166–1169.
 - [43] G.C. Allen, et al., X-ray photoelectron spectroscopy of chromium–oxygen systems, *J. Chem. Soc. Dalton Trans.* 16 (1973) 1675–1683.
 - [44] W.E. Morgan, J.R. Van Wazer, W.J. Stec, Inner-orbital photoelectron spectroscopy of the alkali metal halides, perchlorates, phosphates, and pyrophosphates, *J. Am. Chem. Soc.* 95 (3) (1973) 751–755.
 - [45] M. Zeller, R. Hayes, Evidence from x-ray photoelectron spectroscopy on the charge distribution in various chromium compounds, *Chem. Phys. Lett.* 10 (5) (1971) 610–612.
 - [46] O. Kazushige, et al., Bismuth valence studies of as-grown superconducting Bi-Sr-Ca-Cu-O thin films with T_c(zero) from 98 K to 66 K, *Jpn. J. Appl. Phys.* 31 (7B) (1992) L953.
 - [47] M. Kuba, et al., Mechanism of layer formation on olivine bed particles in industrial-scale dual fluid bed gasification of wood, *Energy Fuel* 30 (9) (2016) 7410–7418.